Sliding Dynamics of Parallel Graphene Sheets: Effect of Geometry and Van Der Waals Interactions on Nano-Spring Behavior

crystals

MDPI

Article

Sliding Dynamics of Parallel Graphene Sheets: Effect of Geometry and Van Der Waals Interactions on Nano-Spring Behavior

Alessandro Crisafulli, Ali Khodayari, Shahin Mohammadnejad and Matteo Fasano *

Energy Department, Politecnico di Torino, Corso Duca degli Abruzzi 24, 10129 Torino, Italy; alessandro.crisafulli@studenti.polito.it (A.C.); ali.khodayari@studenti.polito.it (A.K.); shahin.mohammadnejad@polito.it (S.M.)

* Correspondence: matteo.fasano@polito.it

Received: 15 February 2018; Accepted: 22 March 2018; Published: 28 March 2018

Abstract: Graphene and carbon nanotubes are promising materials for nanoelectromechanical systems. Among other aspects, a proper understanding of the sliding dynamics of parallel graphene sheets or concentric nanotubes is of crucial importance for the design of nano-springs. Here, we analytically investigate the sliding dynamics between two parallel, rigid graphene sheets. In particular, the analysis focuses on configurations in which the distance between the sheets is kept constant and lower than the equilibrium interlayer spacing of graphite (unstable configurations). The aim is to understand how the interlayer force due to van der Waals interactions along the sliding direction changes with the geometrical characteristics of the configuration, namely size and interlayer spacing. Results show metastable equilibrium positions with completely faced sheets, namely a null force along the sliding direction, whereas net negative/positive forces arise when the sheets are approaching/leaving each other. This behavior resembles a molecular spring, being able to convert kinetic into potential energy (van der Waals potential), and viceversa. The amplitude of both storable energy and entrance/exit forces is found to be proportional to the sheet size, and inversely proportional to their interlayer spacing. This model could also be generalized to describe the behavior of configurations made of concentric carbon nanotubes, therefore allowing a rational design of some elements of carbon-based nanoelectromechanical systems.

Keywords: graphene; van der Waals interactions; carbon nanotubes; nanoelectromechanical systems; nano-spring

1. Introduction

Carbon nanotubes (CNTs) and graphene are promising building blocks for nanoelectromechanical systems (NEMS)—such as nanomotors [1,2], nanoprobes [3,4], nanoresistors [5], or nanoswitches [6]—due to their outstanding mechanical [7], electronic [8], and thermal [9–11] properties. In particular, both the telescoping motion between concentric CNTs and multiple layers of graphene (graphite) have shown remarkable ultra-low friction, with almost no hysteresis or dissipation [12–14]. However, a mechanistic understanding of the interaction forces regulating the relative motion of concentric multi-walled carbon nanotubes (MWCNTs) or adjacent graphene sheets is still incomplete.

The sliding motion between concentric CNTs or adjacent graphene sheets is controlled by van der Walls (vdW) interactions [15–17], which depend on the relative position between the nanoconstructs and determine whether they are in a stable, unstable, or metastable configuration. The modern synthesis techniques available in the nanotechnology field allow the production of MWCNTs with precisely controlled chirality and, thus, equilibrium configuration [18–21]. Moreover, the synthesis of

defect-free graphene with a pre-determined number of layers can be precisely achieved by scalable processes based on chemical or shear exfoliation [22–24]. In this context, a stable configuration refers to the state of minimum energy, namely to the relative position leading to the minimum overall interaction potential. In the case of graphite, the global equilibrium distance between its layers (i.e., graphene sheets) is ≈ 0.34 nm [25]. Metastable conditions instead consider stable configurations other than the one corresponding to the system's state of least energy, namely local minimums of van der Walls interaction potential. Finally, unstable configurations refer to relative positions between the nanoconstructs that do not involve either local or global minimums of the overall interaction potential. For example, Cumings et al. [26] experimentally investigated the different energy states of telescoping MWCNTs. In their work, the core of the MWCNT was forced to move through a telescoping cycle inside a housing shell; after that, the inner core was telescoped out by a manipulator, and it was then drawn back into the outer shell by vdW forces to achieve the stable configuration, namely the global minimum of the system's total energy.

The geometry of CNTs and graphene sheets considerably affects their interaction forces, and thus sliding dynamics. First, interaction forces can be dramatically influenced by the effect of commensurability and diameter of nanotubes. Li et al. carried out a series of simulations considering various MWCNTs with a wall spacing of 0.34 nm [27]. The resulting potential energy increments due to the sliding motion between nanotubes indicated that the relative force was independent of the nanotube length and chirality, while these forces were proportional to the diameter of the outer wall of the sliding surface. Similar investigations with capped nanotubes confirmed the dependence of sliding forces with the diameter of CNTs rather than their length [26,28]. Second, the interlayer distance between MWCNTs or graphene sheets also significantly affects their effective vdW interactions. In general, reduced interlayer distances generate higher interlayer friction. This evidence was for example observed by Guo et al. who studied the effect of interlayer distance between graphene sheets by employing molecular force field statistics [29]. Similar results were also reported for capped and uncapped CNTs [30,31].

An interesting characteristic of systems made of MWCNTs or multiple layers of graphene sheets is the pull-out force, namely the force exerted on either inner nanotube pulled out from outer one or on graphene sheets exfoliating each other [27]. In general, the magnitude of the pull-out force depends on the relative distance between nanotubes or graphene layers at the exit position [32]. By considering the direction of sliding motion as a positive reference, pull-out forces are negative for transitions from stable to unstable/metastable conditions (i.e., the sliding motion is energetically unfavorable and an external force is required to pull out the nanoconstruct), while they are positive in the opposite case. Previous works in the literature have mainly focused on the former case, whereas the latter is rather unexplored. However, pull-out forces and sliding dynamics of MWCNTs or multiple layers of graphene sheets are of interest for designing innovative energy accumulators or engines at the molecular scale.

In this work, we analytically investigate the sliding dynamics between two parallel, rigid graphene sheets interacting with each other through van der Waals potential. The aim here is to determine the mechanistic relation between interlayer spacing, sheet size, and the resulting potential energy and pull-out forces along the sliding direction. In particular, the analysis focuses on configurations in which the distance between graphene sheets is kept to less than the equilibrium interlayer spacing of graphite (unstable configurations) in order to achieve higher interaction potentials and thus storable energy. Such configurations could be achieved, for example, when multiple layers of graphene are subject to normal compression [33], and are relevant for a mechanistic understanding of graphite exfoliation as well [34]. In perspective, a generalization of these models can illustrate the interaction forces within MWCNTs as well [35], therefore supporting a more rational design of nanoelectromechanical systems such as nano-springs or actuators.

2. Methods

The analysis aims to study the resulting potential and forces between graphene sheets due to van der Waals interactions, according to different sheet sizes and relative orientation. The 12-6 Lennard-Jones (LJ) potential is used to describe vdW interactions between the atoms of graphene [36], namely

$$V_{LJ}(\mathbf{r}_{ij}) = 4\epsilon \left[\left(\frac{\sigma}{r_{ij}} \right)^{12} - \left(\frac{\sigma}{r_{ij}} \right)^{6} \right] , \tag{1}$$

where $\mathbf{r}_{ij}$ is the distance between i-th and j-th atoms, ϵ is the potential well depth, and σ is the distance at which the interatomic non-bonded potential is zero. In our calculations, $\epsilon = 0.292$ kJ mol^{-1} and $\sigma = 0.35$ nm are considered for carbon atoms, respectively [25,37]. The force due to vdW interactions can be derived from Equation (1) as:

$$\mathbf{F}_{LJ}(\mathbf{r}_{ij}) = 4\epsilon \left[12 \left(\frac{\sigma^{12}}{r_{ij}^{13}} \right) - 6 \left(\frac{\sigma^{6}}{r_{ij}^{7}} \right) \right] \frac{\mathbf{r}_{ij}}{r_{ij}} . \tag{2}$$

The interatomic distance at which the potential reaches its lowest value ($-\epsilon$) can be computed as $r_m = 2^{1/6}\sigma \approx 1.122\sigma$, being $F_{LJ}(r_m) = 0$. Note that this distance is equal to $r_m = 0.39$ nm in the case of carbon-carbon interactions. For the sake of simplicity, some assumptions have been made for the sliding motion of the considered configurations, namely: one nanostructure is fixed while the other one is moving; the sliding motion occurs along one single axis at time; graphene sheets are assumed to be perfectly rigid and flat (with no defects); and no relative motion between atoms of the same plane is considered (consequently, intraplane forces are neglected). The calculations of the resulting LJ forces and potentials are performed through a MATLAB® code (see a representative example in Appendix A).

Four configurations have been considered in the following analysis, with increasing degrees of complexity. Figure 1a shows the first studied configuration, which contains one atom with a fixed position ($x = 0$) and another one moving along the x direction. The normal distance between the two atoms is kept constant at a fixed distance $\Delta Z = 0.28$ or 0.34 nm, in order to investigate its effect on interatomic vdW forces. As for the second configuration, the dynamics of a carbon atom sliding over a fixed chain of carbon atoms is studied, as depicted in Figure 1b. Herein, the atoms of the chain are separated by $b = 0.246$ nm, that is, the distance between two hexagonal lattices of graphene. The third configuration is depicted in Figure 1c, with two chains of carbon atoms at the ΔZ distance sliding over each other along x axis. Note that in the second and third configurations, the first atom of the fixed chain is positioned at $x = 0$. The fourth configuration considers two graphene sheets at ΔZ distance (Figure 1d), the hexagonal lattice of graphene being characterized by $a = 0.142$ nm (C-C bond length) and $b = 0.246$ nm characteristic sizes [25,38]. Accordingly, the size (L_x, L_y) and number of atoms (N_a) of each graphene sheet can be computed as

$$L_x = a \cdot h_x + 2a \cdot (h_x - 1) \quad (\text{nm}) , \tag{3}$$

$$L_y = b \cdot h_y \quad (\text{nm}) , \tag{4}$$

$$N_a = 2h_x \left[3 + 2(h_y - 1) \right] , \tag{5}$$

where h_x and h_y refer to the number of hexagonal lattices in the related direction. In the following analyses, the size of stationary graphene sheet is fixed at $h_x = h_y = 7$ ($L_x = 2.7$ nm, $L_y = 1.722$ nm, 210 atoms). The size of the sliding sheet is varied to assess possible size effects (see Table 1 for a detailed list of considered configurations).

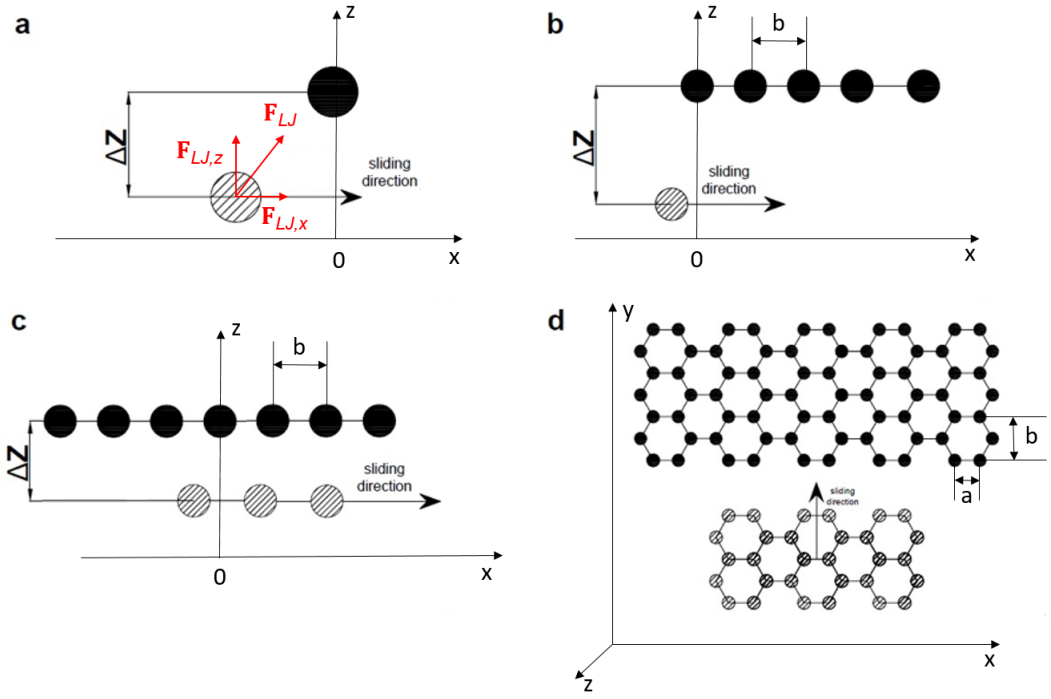

Figure 1. Sliding configurations: black dots represent fixed carbon atoms, while dashed dots represent sliding ones. (**a**) A pair of sliding atoms; (**b**) An atom slides over a chain of atoms; (**c**) A pair of sliding chains of atoms; (**d**) A pair of graphene sheets at ΔZ distance sliding along the y direction. The resulting LJ forces and potentials between the carbon-based nanostructures have been computed to assess the effect of interlayer spacing and structure size on the sliding dynamics of each configuration.

Table 1. Considered geometrical configurations of the sliding graphene sheet (dashed atoms in Figure 1d).

h_x	h_y	L_x (nm)	L_y (nm)	N_a
2	3	0.568	0.738	28
2	4	0.568	0.984	36
2	5	0.568	1.230	44
3	4	0.994	0.984	54
3	5	0.994	1.230	66

Note that in most considered cases, the interlayer distance between graphene sheets (ΔZ) is chosen to be lower than the stable equilibrium value. This is in order to investigate a compressed configuration between the two graphene sheets and thus metastable equilibrium conditions. Such a configuration is preferred for implementing the proposed concept of the nano-spring. To this end, we arbitrarily decide to consider $\Delta Z = 0.28$ in the following analyses; however, any choice of $\Delta Z < 0.34$ nm would have led to similar results and conclusions (even if with different absolute values of Lennard-Jones interactions and forces).

3. Results and Discussion

3.1. Atom–Atom Sliding

In Figure 2, the van der Waals potential and interatomic force between the pair of atoms in Figure 1a are first presented. These carbon atoms are supposed to slide over each other along the x

direction, and the study is replicated for different ΔZ. It is noteworthy to mention that, herein, the force along x axis ($F_{LJ,x}$) is considered as positive when it is concordant with the direction of sliding.

In Figure 2a, the normal distance between carbon atoms is $\Delta Z = 0.34$ nm, which is approximately equal to the equilibrium interlayer distance of graphite. Results highlight the presence of two symmetrical stable equilibrium positions (i.e., $x \approx \pm 0.2$ nm), where V_{LJ} is the minimum and $F_{LJ,x} = 0$. Moreover, when the sliding atom is positioned at $x = 0$—that is the position where the two atoms are facing each other with respect to x axis—$F_{LJ,x} = 0$ and V_{LJ} is the maximum (unstable equilibrium). A similar behavior is observed with $\Delta Z = 0.28$ nm (Figure 2b, two symmetrical stable equilibrium positions at $x \approx \pm 0.25$ nm); however, the shorter normal distance between atoms leads to stronger vdW interactions and, thus, up to one order of magnitude larger potential and force peaks.

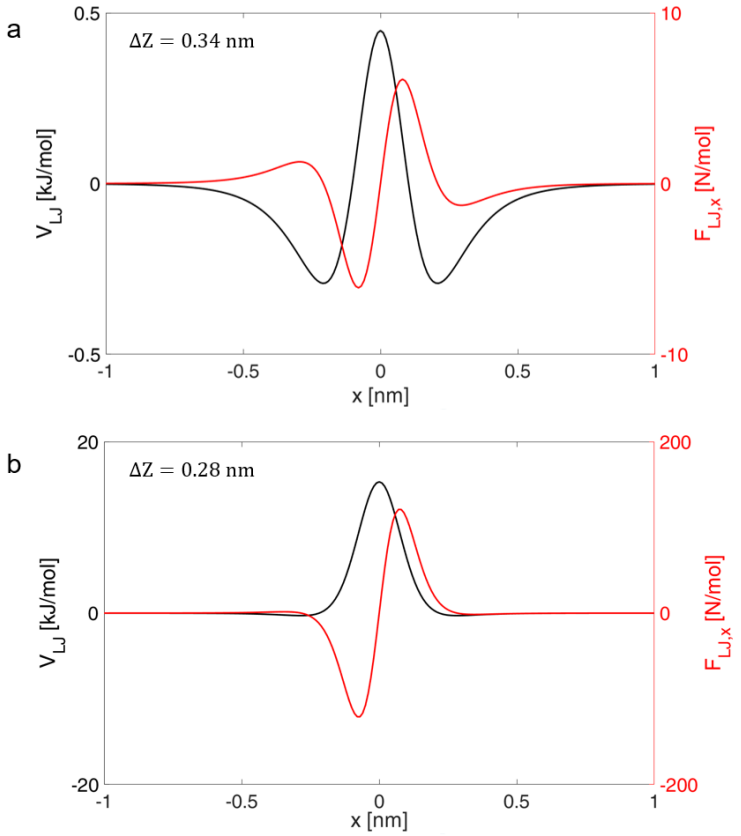

Figure 2. Interatomic van der Walls (vdW) potential (black lines) and force along the x direction (red lines) between two atoms of carbon (see configuration in Figure 1a), for (**a**) $\Delta Z = 0.34$ nm and (**b**) $\Delta Z = 0.28$ nm.

3.2. Atom–Chain Sliding

Second, Figure 3 depicts the resulting potential and force between one atom sliding over a fixed chain of atoms ($N_a = 5$, see configuration in Figure 1b). In this case, the distance between the chain and the sliding atom is kept constant at $\Delta Z = 0.28$ nm; however, results could be eventually generalized according to what has been discussed in the previous section.

In particular, each colored line in Figure 3a corresponds to the vdW potential between the sliding atom and one specific atom in the stationary chain. Coherently with the results reported in Figure 2b, these atom–atom potentials present two symmetrical stable equilibrium positions (global minimum of potential) and an unstable one (potential peak). The effective potential between the sliding atom and the stationary chain is then computed through the superimposition of the five atom–atom interactions (dashed line in Figure 3a). Figure 3b, instead, provides the force exerted by the carbon chain on the

sliding atom along x direction. The effective force (dashed line) and the contribution given by the first atom of the chain (colored line) are both reported, with trends in agreement with Figure 2b.

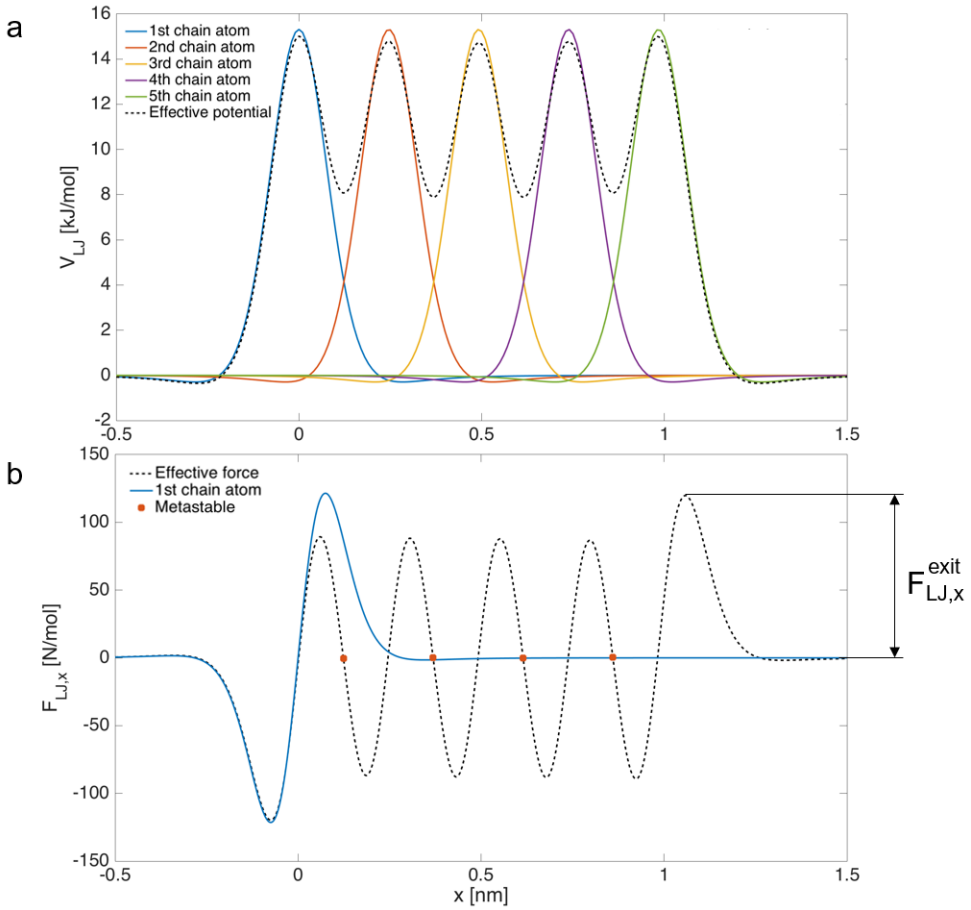

Figure 3. (**a**) Interatomic vdW potential between one carbon atom and a chain of carbon atoms. The effective potential (dashed line) is computed from the superimposition of all interactions between the sliding atom and the atoms of the stationary chain (colored lines); (**b**) VdW force exerted by the carbon chain on the sliding atom along the x direction: the effective force (dashed line) and contribution given by the first atom of the chain (colored line). Orange dots correspond to metastable equilibrium positions.

The effective force between the sliding atom and the chain oscillates periodically between positive and negative peaks. These peaks are lower than those given by single atom–atom interactions, due to the superimposition of effects of neighbor atoms. Note that the sliding atom is subject to a force with larger amplitude when passing the last atom; this force can be named the pull-out or exit force ($F^{exit}_{LJ,x}$). In this case, the exit force is also the maximum effective force measured along the sliding motion.

During the sliding motion, a null effective force is recovered in two periodical conditions: (1) the sliding atom faces a fixed atom of the chain ($x = kb$, with $0 \leq k \leq (N_a - 1)$); and (2) the sliding atom is located halfway between two atoms of the chain ($x = b/2 + kb$, with $0 \leq k \leq (N_a - 2)$). The former cases correspond to unstable equilibrium positions (effective potential peaks), while the latter cases correspond to metastable equilibrium positions (local minimums of effective potential, orange dots in Figure 3b). In addition, stable equilibrium positions are still noticeable at $x \approx -0.25$ nm and $x \approx 1.3$ nm, where the sliding atom enters or exits the carbon chain, respectively. Note that the very slight ≈0.1 Å offset of these equilibrium positions with respect to the previous atom–atom configuration is due to the superimposition of Van der Waals potential from the other atoms of the fixed chain. In fact, considering for example the equilibrium position at the chain entrance ($x \approx -0.25$ nm),

an almost perfect overlap between the effective LJ potential—dashed black line—and the LJ potential between the sliding atom and the first atom of the chain—solid blue line—can be observed in Figure 3a. Similar discussions could be argued for the sliding atom leaving the proximity of the chain, namely for the second equilibrium position at $x \approx 1.3$ nm.

3.3. Chain–Chain Sliding

Third, the sliding motion between two chains of carbon atoms is investigated (configuration in Figure 1c): the fixed and sliding chains are made of $N_a = 7$ and 3 atoms, respectively. In accordance with the previous setups, the normal distance between the chains is equal to $\Delta Z = 0.28$ nm.

The potential between each atom of the sliding chain and the fixed ones is reported in Figure 4a, with trends similar to the atom–chain case. The resulting effective potential highlights again the presence of stable, metastable and unstable equilibrium positions throughout the motion of the sliding chain over the stationary one. In particular, the two stable equilibrium positions are still observable with chains separated 0.25 nm from each other along the x axis. Conversely, unstable and metastable equilibrium positions appear with overlapping chains. Again, unstable equilibrium positions are associated with atom-atom facing, while metastable equilibrium positions emerge with alternated atoms, with periodicity determined by the chain lattice b.

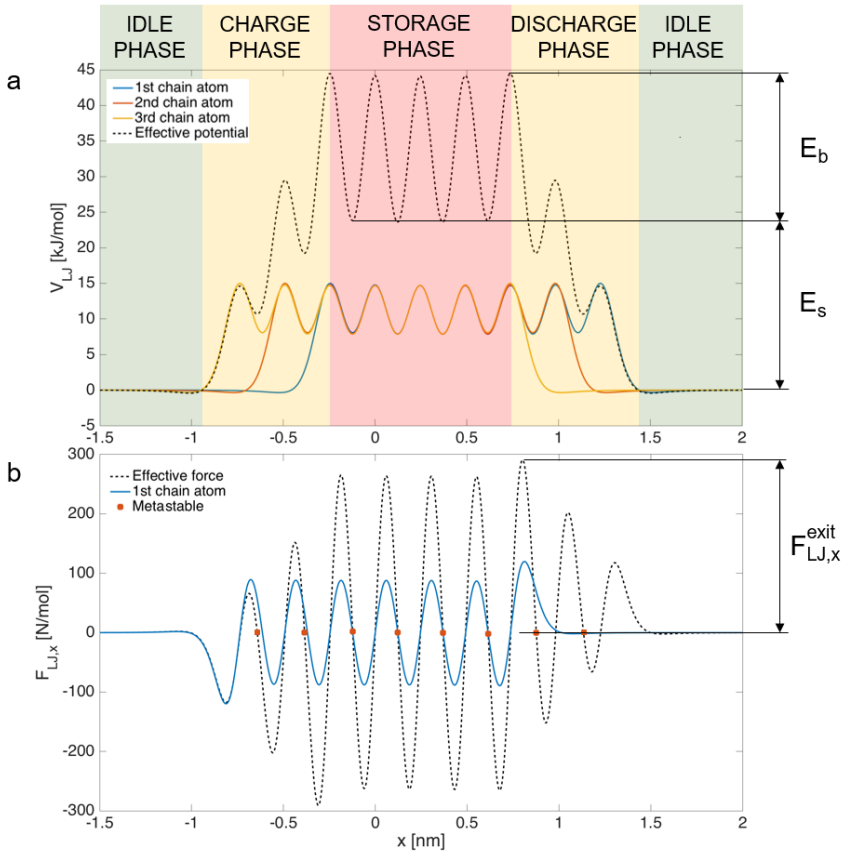

Figure 4. (**a**) Interatomic vdW potential between two chains of carbon atoms. The effective potential (dashed line) is computed from the superimposition of all the interactions between each atom of the sliding and the stationary chains (colored lines); (**b**) VdW force exerted by the stationary chain on the sliding one along the x direction: effective force (dashed line) and contribution given by the first atom of the sliding chain (colored line). Orange dots correspond to metastable equilibrium positions.

Results show that the effective potential exerted on the sliding chain by the stationary one (dashed line in Figure 4a) scales approximately linearly with the number of sliding atoms that overlook the

stationary chain. A similar behavior of $F_{LJ,x}$ is also observed (dashed line in Figure 4b). Of note, the largest amplitude of force opposite to the sliding motion shows up when the last atom of the sliding chain fully enters the stationary chain. The largest amplitude of force coherent with the sliding motion corresponds to the pull-out force ($F_{LJ,x}^{exit}$). Clearly, the amplitude of vdW forces depends on the size of the sliding chain, since a higher number of interacting atoms leads to a stronger vdW potential by superimposition of effects. This is totally coherent with the macroscopic friction between two surfaces.

Therefore, the sliding chain requires an initial amount of energy to move from stable (separated chains) to metastable (overlapped chains) equilibrium positions, with an energy barrier ($E_b + E_s$, see Figure 4a) determined by the potential peak $V_{LJ} = 45$ kJ/mol. After this entrance phase, the sliding chain stabilizes in the metastable equilibrium positions, where part of the initial energy input is accumulated in the form of vdW potential energy. Such stored energy ($E_s = 25$ kJ/mol) can be released back after the pull-out phase, when a stable equilibrium position between the chains is eventually achieved. Clearly, E_s scales with the number of atoms in the sliding element, because of the superimposition of their vdW interaction energies. As highlighted in Figure 4a, this cycle resembles the behavior of nano-springs, where kinetic energy can be iteratively converted and stored in the form of potential energy, namely vdW interactions in this case. These alternate charge/discharge phases are possible thanks to the sliding motion between the two carbon chains. Note that since the energy storage phase takes place in the metastable equilibrium positions, the discharge phase is not spontaneous, but must be triggered by overcoming an energy barrier approximately equal to $E_b = 20$ kJ/mol.

3.4. Sheet–Sheet Sliding

The sliding motion between the two graphene sheets depicted in Figure 1d is finally analyzed. Initially, the stationary sheet consists of 210 atoms ($h_x = h_y = 7$), while the sliding sheet consists of 30 atoms ($h_x = 3$, $h_y = 2$). Interaction potential and effective force are calculated for interlayer spacings equal to $\Delta Z = 0.28$ nm or $\Delta Z = 0.34$ nm, in order to consider either unstable or stable configurations, respectively. The sliding motion of the sheets is only analyzed along the y axis; nevertheless, similar results could be obtained for the x axis motion as well.

Figure 5 displays $F_{LJ,y}$ and V_{LJ} exerted by the stationary graphene sheet on the sliding one along the y direction. By comparing the results in Figure 5a ($\Delta Z = 0.34$ nm) with the ones in Figure 5b ($\Delta Z = 0.28$ nm), a dramatically different behavior and magnitude of the effective potential and force between the sheets can be noticed.

On the one side, in the $\Delta Z = 0.34$ nm case, the sliding graphene sheet meets a global minimum of V_{LJ} (stable equilibrium) in the middle of the stationary sheet. Hence, the moving sheet naturally tends to slide over the stationary one until a complete overlap is achieved. A net input energy should be provided to exfoliate them. Such a self-retracting motion of sheared graphene sheets back to a piled configuration under no external influences (i.e. only driven by the van der Waals forces within the system) has been confirmed by several studies in the literature [39]. For example, Liu et al. measured the interlayer shear strength of few layers of graphene (single crystalline graphite) covered by SiO_2 square mesas, with an overall height of 100–500 nm [40]. A micro-manipulator equipped with a micro-tip was then employed to apply a shear force on the SiO_2 top surface of the mesa and thus on the graphite layers. In agreement with our results for $\Delta Z = 0.34$ nm, the sheared sheets were observed to spontaneously move back to their previous position, a stable equilibrium one.

On the other hand, in the $\Delta Z = 0.28$ nm case and similarly to the simpler configurations discussed in the previous sections, the two graphene sheets undergo a series of different equilibrium conditions throughout their relative sliding motion along the y axis. In fact, while stable equilibrium is achieved with separated sheets, unstable and metastable equilibrium positions are again observed with overlapping sheets. In this case, when the sliding sheet is completely contained in the stationary one, the position of metastable equilibrium points is periodic with the characteristic size of the graphene lattice along the sliding direction, namely b. Clearly, the edge termination determines the position of the pull-out (exit) force. As an example, in Figure 5b, the exit force manifests at $y \approx 1.3$ nm: when the

edges of the sliding and the stationary sheet coincide, each sheet experiences an exit force equal to $F_{LJ,y}^{exit}$. Therefore, in the nano-spring concept discussed in this article, the graphene edges introduce the energy barriers required for storing energy in the form of vdW potential, namely for keeping the sheets under metastable equilibrium conditions. The metastable equilibrium positions, which show an average interaction potential equal to $E_s \approx 430$ kJ/mol, are achieved after that the energy barrier $E_b + E_s = 550$ kJ/mol is overcome. These potential energy values are one order of magnitude larger than the ones observed for the sliding motion of chains of carbon atoms, because of the increased number of interacting atoms.

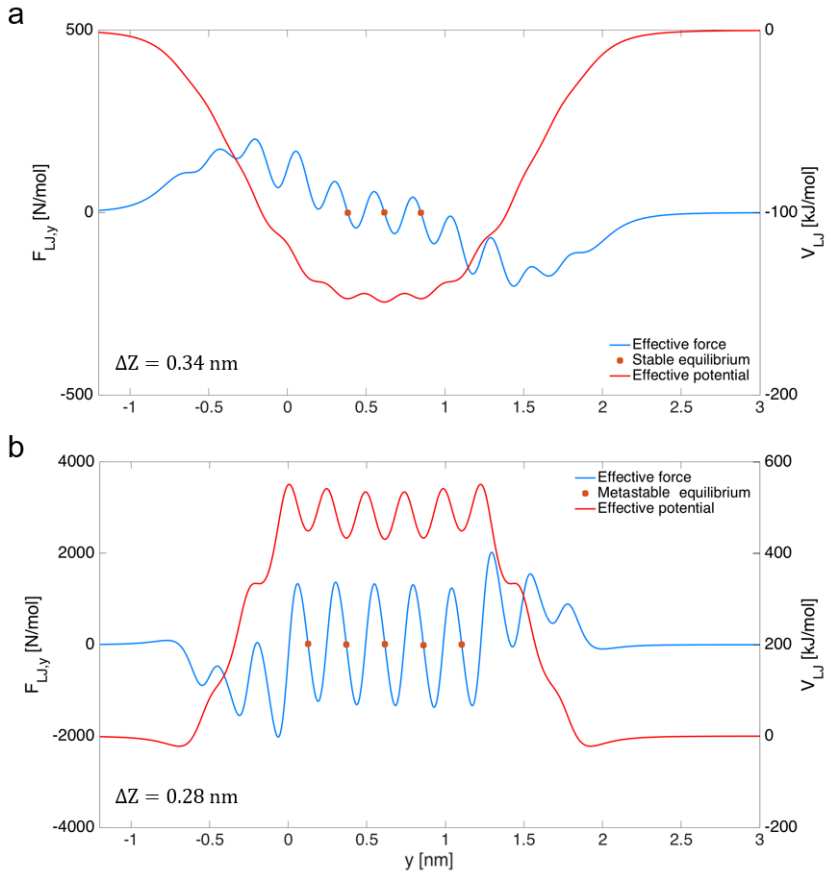

Figure 5. VdW potential (red lines) and effective force (blue lines) exerted by the stationary graphene sheet on the sliding one along the y direction. The two sheets are either (**a**) $\Delta Z = 0.34$ nm or (**b**) $\Delta Z = 0.28$ nm apart from each other. Orange dots correspond to either stable or metastable equilibrium positions, respectively.

To increase the generality of such evidence, a sensitivity analysis has been carried out to assess the effect of both sliding sheet size (N_a) and interlayer spacing (ΔZ) on the energy barrier (E_b, Figure 6a), storable energy (E_s, Figure 6b), and exit force ($F_{LJ,y}^{exit}$, Figure 6c) of two graphene sheets sliding along the y direction. Results show that E_b, E_s, and $F_{LJ,y}^{exit}$ tend to increase with lower ΔZ following a power law, because of the enhanced vdW interactions at shorter distances (see Equations (1) and (2)). Furthermore, as reported in the insets for a fixed $\Delta Z = 0.28$ nm (although similar trends can be found with different ΔZ), E_b, E_s, and $F_{LJ,y}^{exit}$ linearly increase with N_a. Such behavior is coherent with the superimposition of vdW interactions between the atoms of the sliding and stationary sheets. Note that the slight deviations from this linear trend may be due to the different shape of the sliding sheets (h_x, h_y).

Figure 6d sketches a conceptual scheme of two sliding graphene sheets at fixed ΔZ that are employed as a nano-spring. The purpose is to convert kinetic into potential energy, store it, and then

release it after the application of an external trigger. In detail, in the case of unstable configurations (i.e., $\Delta Z < 0.34$ nm), the sliding sheet moves from stable (separated sheets) to metastable (overlapped sheets) equilibrium positions after an external energy input ($E_s + E_b$). After that, the sliding sheet is entrapped in the metastable equilibrium positions and, thus, energy is stored in the form of vdW potential energy (E_s) for an indefinite amount of time. The application of an additional amount of external energy (E_b), which is lower than the stored energy, triggers the pull-out phase of the sliding sheet and thus releases back the accumulated energy. Clearly, similar nano-spring cycles could be also envisioned for stable configurations of graphene sheets (i.e., $\Delta Z \approx 0.34$ nm), even though the reduced vdW interactions would imply a lower storable energy.

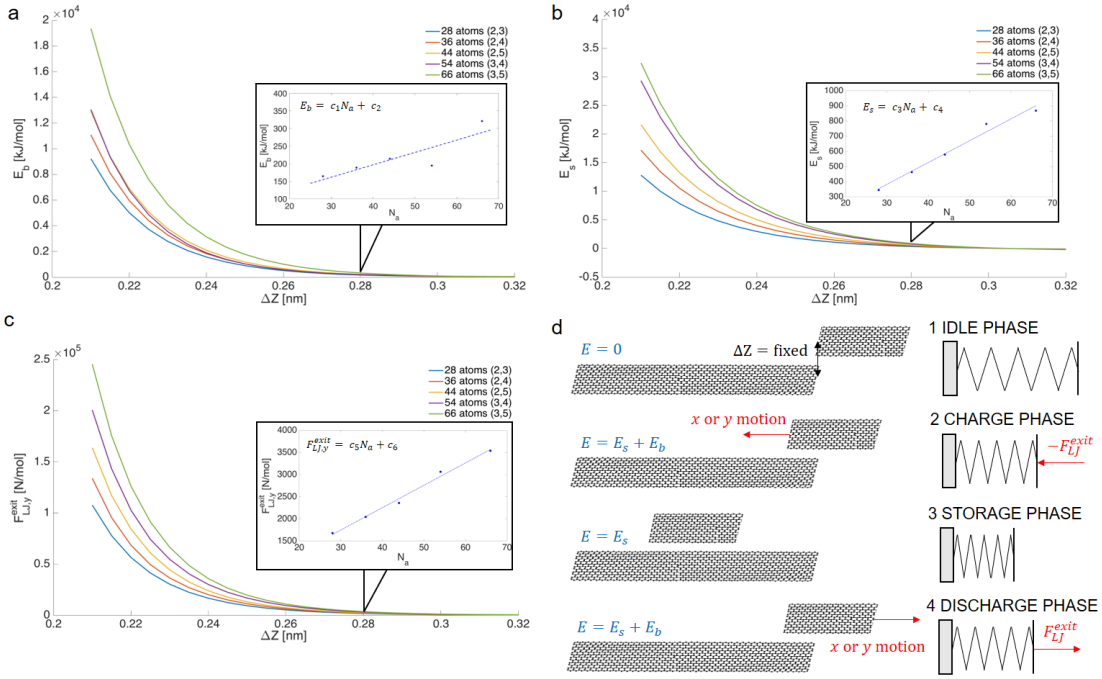

Figure 6. (**a**) Energy barrier, E_b; (**b**) storable energy, E_s; and (**c**) exit force, $F^{exit}_{LJ,y}$ for pairs of sliding graphene sheets at a different normal distance (ΔZ). Various sizes of the sliding sheet are also considered (colored lines). Note that the considered direction of sliding is along the y axis. In the insets, the trend of E_b, E_s, and $F^{exit}_{LJ,y}$ at fixed $\Delta Z = 0.28$ nm and with different numbers of atoms of the sliding sheet (N_a) is represented. The coefficients of the linear fittings in the insets are equal to $c_1 = 3.5$ kJ/mol, $c_2 = 56.1$ kJ/mol, $c_3 = 14.4$ kJ/mol, $c_4 = -50.5$ kJ/mol, $c_5 = 50.5$ N/mol, and $c_6 = 232.8$ N/mol; (**d**) Conceptual scheme of a nano-spring made of two sliding graphene sheets.

A configuration where graphene sheets present an interlayer distance lower than the stable equilibrium distance could be achieved by applying a fixed compression force normal to the stacked sheets. For example, experiments aiming to investigate the sliding motion between graphene sheets under metastable conditions as depicted in Figure 6d could be organized in the following steps: (1) generation of double layers of graphene (or graphene oxide), for instance by Langmuir-Blodgett assembly [41]; (2) compression of the double layers of graphene by means of a nano-indenter [42]; and (3) measurement of the forces occurring during the sliding dynamics by means of a nano-manipulator [26]. Note that characterization techniques such as atomic force microscopy (AFM) or in situ Raman mapping [43], as well as atomistic simulations [44,45], could support the experimental implementation and analysis of this system. Finally, the nano-spring concept outlined in this article could also be implemented and validated by experiments with systems made of multi-walled carbon nanotubes under telescopic motion [26].

4. Conclusions

A mechanistic understanding of the exfoliation and tribology of carbon nanotubes and graphene sheets is required for the precise fabrication of nanoelectromechanical systems. In particular, the performance of such devices can be enhanced by achieving a proper knowledge of the interlayer sliding dynamics between graphene sheets or nanotubes.

In this work, the interatomic interactions between two parallel, rigid graphene sheets were analytically investigated. While prior works were mainly focused on analyzing the behavior of graphene sheets with stable interlayer spacing, we studied a simple model of two graphene sheets sliding over each other under unstable conditions as well. Such far-from-equilibrium interlayer distances may be exploited to realize molecular nano-springs, namely nanostructures that allow us to accumulate, store and then release kinetic energy, thanks to the variation in potential energy (vdW interactions). Our results highlight a precise pattern of relative positions between graphene sheets leading to metastable equilibrium conditions. Moreover, the amplitude of the effective potential and forces between the sheets is proportional to their size, while it is inversely proportional to the interlayer spacing. This regulates the amount of energy that could be potentially accumulated in a possible nano-spring application of pairs of graphene sheets or multi-walled carbon nanotubes.

Further investigations should be devoted to the effect of vibrational energy on the aforementioned results, for example by studying similar configurations through molecular dynamics simulations. In perspective, this analysis could be extended to multi-walled carbon nanotubes, in order to provide a more generalized view of the design of nano-springs for engineering or biomedical applications.

Acknowledgments: The authors are grateful to the financial support by Politecnico di Torino through the RTDa Starting Grant 56_RIL16FAM01. This work has partially received funding from the European Union's Horizon 2020 research and innovation program MODCOMP under grant agreement NO. 685844.

Author Contributions: M.F. conceived and designed the study; A.C. and A.K. performed the calculations; M.F., A.K. and S.M. analyzed the data; all authors contributed to the writing of the paper.

Conflicts of Interest: The authors declare no conflict of interest.

Appendix A

Code to compute Lennard-Jones potential and forces between sliding sheets of graphene at given normal distance.

```
%% Input parameters (editable)
a0=0.1421; % graphene lattice [nm]
a1=a0*sin(pi/6); % graphene lattice [nm]
a2=a0*cos(pi/6); % half height of the graphene lattice [nm]
a3=2*a1+a0; % maximum distance in graphene lattice [nm]
hxf=7; % number of hexagons in x direction for the fixed sheet
hyf=7; % number of hexagons in y direction for the fixed sheet
hxs=3; % number of hexagons in x direction for the sliding sheet
hys=2; % number of hexagons in y direction for the sliding sheet
s=3;   % shift of sliding sheet along x direction
DeltaZ=0.28; % interplanar distance [nm]
sigma=0.355; % LJ radius of carbon [nm]
epsilon=0.292288; % LJ potential well of carbon [kJ/mol]

%% Generation of the Fixed Sheet
p1=zeros(1,2*hxf);
p1(1)=a1;
for i=2:2*hxf
    if mod(i,2)==0
```

```
        p1(i)=p1(i-1)+a0;
    else
        p1(i)=p1(i-1)+a3;
    end
end
p2=[0,p1(1:end-1)+a0+a1];
nf=2*hyf+1;
for i=1:nf
    if mod(i,2)==0
        FP(1+(i-1)*length(p1):i*length(p1),1)=p2;
    else
        FP(1+(i-1)*length(p1):i*length(p1),1)=p1;
    end
    FP(1+(i-1)*length(p1):i*length(p1),2)=[(i-1)*a2];
end

%% Generation of the Sliding Sheet
p1=zeros(1,2*hxs);
p1(1)=a1;
for i=2:2*hxs
    if mod(i,2)==0
        p1(i)=p1(i-1)+a0;
    else
        p1(i)=p1(i-1)+a3;
    end
end
p2=[0,p1(1:end-1)+a0+a1];
ns=2*hys+1;
for i=1:ns
    if mod(i,2)==0
        SP(1+(i-1)*length(p1):i*length(p1),1)=p2;
    else
        SP(1+(i-1)*length(p1):i*length(p1),1)=p1;
    end
    SP(1+(i-1)*length(p1):i*length(p1),2)=[(i-1)*a2];
end
SP(:,1)=SP(:,1)+s*(a0+a3);

%% LJ Force and Potential Calculation (during sliding motion)
step=[-1.2:0.001:3];
LJ_P=zeros(length(step),length(SP));
LJ_FY=zeros(length(step),length(SP));
for t=1:length(step)
    for j=1:length(FP)
        for i=1:length(SP)
    R=sqrt((SP(i,1)-FP(j,1))^2+(SP(i,2)+step(t)-FP(j,2))^2+DeltaZ^2);
    LJ_P(t,i)=4*epsilon*((sigma/R)^12-(sigma/R)^6)+LJ_P(t,i);
    LJ_FY(t,i)=4*epsilon*(12*(sigma^12)/(R^13)-6*(sigma^6)/(R^7))*(SP(i,2)+...
        step(t)-FP(j,2))/R+LJ_FY(t,i);
        end
```

```
    end
end
FY=sum(LJ_FY,2); % Interatomic force [N/mol]
LJ=sum(LJ_P,2); % Lennard-Jones potential [kJ/mol]
```

References

1. Bailey, S.W.D.; Amanatidis, I.; Lambert, C.J. Carbon nanotube electron windmills: A novel design for nanomotors. *Phys. Rev. Lett.* **2008**, *100*, 256802.
2. Laocharoensuk, R.; Burdick, J.; Wang, J. Carbon-nanotube-induced acceleration of catalytic nanomotors. *ACS Nano* **2008**, *2*, 1069–1075.
3. Hui, F.; Chen, S.; Liang, X.; Yuan, B.; Jing, X.; Shi, Y.; Lanza, M. Graphene Coated Nanoprobes: A Review. *Crystals* **2017**, *7*, 269.
4. Kazakova, O.; Panchal, V.; Burnett, T.L. Epitaxial graphene and graphene–based devices studied by electrical scanning probe microscopy. *Crystals* **2013**, *3*, 191–233.
5. Cumings, J.; Zettl, A. Localization and nonlinear resistance in telescopically extended nanotubes. *Phys. Rev. Lett.* **2004**, *93*, 086801.
6. Deshpande, V.; Chiu, H.Y.; Postma, H.C.; Miko, C.; Forro, L.; Bockrath, M. Carbon nanotube linear bearing nanoswitches. *Nano Lett.* **2006**, *6*, 1092–1095.
7. Yu, M.F.; Yakobson, B.I.; Ruoff, R.S. Controlled sliding and pullout of nested shells in individual multiwalled carbon nanotubes. *J. Phys. Chem. B* **2000**, *104*, 8764–8767.
8. Collins, P.G.; Arnold, M.S.; Avouris, P. Engineering carbon nanotubes and nanotube circuits using electrical breakdown. *Science* **2001**, *292*, 706–709.
9. Bigdeli, M.B.; Fasano, M. Thermal transmittance in graphene based networks for polymer matrix composites. *Int. J. Therm. Sci.* **2017**, *117*, 98–105.
10. Fasano, M.; Bigdeli, M.B.; Sereshk, M.R.V.; Chiavazzo, E.; Asinari, P. Thermal transmittance of carbon nanotube networks: Guidelines for novel thermal storage systems and polymeric material of thermal interest. *Renew. Sustain. Energy Rev.* **2015**, *41*, 1028–1036.
11. Fasano, M.; Bigdeli, M.B. Bottom up Approach Toward Prediction of Effective Thermophysical Properties of Carbon-Based Nanofluids. *Heat Transf. Eng.* **2017**, pp. 1–12, doi:10.1080/01457632.2017.1384283.
12. Kis, A.; Jensen, K.; Aloni, S.; Mickelson, W.; Zettl, A. Interlayer Forces and Ultralow Sliding Friction in Multiwalled Carbon Nanotubes. *Phys. Rev. Lett.* **2006**, *97*, 025501.
13. Dienwiebel, M.; Verhoeven, G.S.; Pradeep, N.; Frenken, J.W.; Heimberg, J.A.; Zandbergen, H.W. Superlubricity of graphite. *Phys. Rev. Lett.* **2004**, *92*, 126101.
14. Dienwiebel, M.; Pradeep, N.; Verhoeven, G.S.; Zandbergen, H.W.; Frenken, J.W. Model experiments of superlubricity of graphite. *Surf. Sci.* **2005**, *576*, 197–211.
15. He, X.Q.; Kitipornchai, S.; Liew, K.M. Buckling analysis of multi-walled carbon nanotubes: A continuum model accounting for van der Waals interaction. *J. Mech. Phys. Solids* **2005**, *53*, 303–326.
16. Girifalco, L.A.; Hodak, M.; Lee, R.S. Carbon nanotubes, buckyballs, ropes, and a universal graphitic potential. *Phys. Rev. B* **2000**, *62*, 104–110.
17. Cui, Z.; Guo, J.G. Theoretical investigations of the interfacial sliding and buckling of graphene on a flexible substrate. *AIP Adv.* **2016**, *6*, 125110.
18. Briggs, N.; Crossley, S. Rapid growth of vertically aligned multi-walled carbon nanotubes on a lamellar support. *RSC Adv.* **2015**, *5*, 83945–83952.
19. Krasnikov, D.; Shmakov, A.; Kuznetsov, V.; Ishchenko, A. Towards the optimization of carbon nanotube properties via in situ and ex situ studies of the growth mechanism. *J. Struct. Chem.* **2016**, *57*, 1436–1443.
20. Li, Y.j.; Ma, C.; Kang, J.l.; Shi, J.l.; Shi, Q.; Wu, D.h. Preparation of diameter-controlled multi-wall carbon nanotubes by an improved floating-catalyst chemical vapor deposition method. *N. Carbon Mater.* **2017**, *32*, 234–241.
21. Gallego, J.; Barrault, J.; Batiot-Dupeyrat, C.; Mondragon, F. Intershell spacing changes in MWCNT induced by metal–CNT interactions. *Micron* **2013**, *44*, 463–467.
22. Wu, Z.S.; Ren, W.; Gao, L.; Liu, B.; Jiang, C.; Cheng, H.M. Synthesis of high-quality graphene with a pre-determined number of layers. *Carbon* **2009**, *47*, 493–499.

23. Paton, K.R.; Varrla, E.; Backes, C.; Smith, R.J.; Khan, U.; O'Neill, A.; Boland, C.; Lotya, M.; Istrate, O.M.; King, P.; et al. Scalable production of large quantities of defect-free few-layer graphene by shear exfoliation in liquids. *Nat. Mater.* **2014**, *13*, 624.
24. Hadi, A.; Zahirifar, J.; Karimi-Sabet, J.; Dastbaz, A. Graphene nanosheets preparation using magnetic nanoparticle assisted liquid phase exfoliation of graphite: The coupled effect of ultrasound and wedging nanoparticles. *Ultrason. Sonochem.* **2018**, *44*, 204–214.
25. Delhaes, P. *Graphite and Precursors*; CRC Press: Boca Raton, FL, USA, 2000.
26. Cumings, J.; Zettl, A. Low-Friction Nanoscale Linear Bearing Realized from Multiwall Carbon Nanotubes. *Science* **2000**, *289*, 602–605.
27. Li, Y.; Hu, N.; Yamamoto, G.; Wang, Z.; Hashida, T.; Asanuma, H.; Dong, C.; Okabe, T.; Arai, M.; Fukunaga, H. Molecular mechanics simulation of the sliding behavior between nested walls in a multi-walled carbon nanotube. *Carbon* **2010**, *48*, 2934–2940.
28. Yamamoto, G.; Liu, S.; Hu, N.; Hashida, T.; Liu, Y.; Yan, C.; Li, Y.; Cui, H.; Ning, H.; Wu, L. Prediction of pull-out force of multi-walled carbon nanotube (MWCNT) in sword-in-sheath mode. *Comput. Mater. Sci.* **2012**, *60*, 7–12.
29. Guo, Y.; Guo, W.; Chen, C. Modifying atomic-scale friction between two graphene sheets: A molecular-force-field study. *Phys. Rev. B* **2007**, *76*, 155429, doi:10.1103/PhysRevB.76.155429.
30. Xia, Z.; Curtin, W.A. Pullout forces and friction in multiwall carbon nanotubes. *Phys. Rev. B* **2004**, *69*, 1–4.
31. Guo, W.; Gao, H. Optimized bearing and interlayer friction in multiwalled carbon nanotubes. *CMES Comput. Model. Eng. Sci.* **2005**, *7*, 19–34.
32. Kimoto, Y.; Mori, H.; Mikami, T.; Akita, S.; Nakayama, Y.; Higashi, K.; Hirai, Y. Molecular Dynamics Study of Double-Walled Carbon Nanotubes for Nano-Mechanical Manipulation. *Jpn. J. Appl. Phys.* **2005**, *44*, 1641–1647.
33. Shakouri, A.; Yeo, J.; Ng, T.Y.; Liu, Z.; Taylor, H. Superlubricity-activated thinning of graphite flakes compressed by passivated crystalline silicon substrates for graphene exfoliation. *Carbon* **2014**, *80*, 68–74.
34. Sung, M.K.; Lee, S. The Effect of van der Waals Forces on the Exfoliation of Graphene Sheets from Graphite by Frictional Motion. *J. Nanosci. Nanotechnol.* **2016**, *16*, 11529–11534.
35. Tanaka, K.; Aoki, H. Interlayer interaction of two graphene sheets as a model of double-layer carbon nanotubes. *Carbon* **1997**, *35*, 121–125.
36. Silva, F.R.; Filho, E.D. Confined Lennard Jones potential: a variational treatment. *Mod. Phys. Lett. A* **2010**, *25*, 641–648.
37. Kaukonen, M.; Gulans, A.; Havu, P.; Kauppinen, E. Lennard-Jones parameters for small diameter carbon nanotubes and water for molecular mechanics simulations from van der Waals density functional calculations. *J. Comput. Chem.* **2012**, *33*, 652–658.
38. Kis, A.; Zettl, A. Nanomechanics of carbon nanotubes. *Philos. Trans. R. Soc. A* **2008**, *366*, 1591–1611.
39. Zheng, Q.; Jiang, B.; Liu, S.; Weng, Y.; Lu, L.; Xue, Q.; Zhu, J.; Jiang, Q.; Wang, S.; Peng, L. Self-retracting motion of graphite microflakes. *Phys. Rev. Lett.* **2008**, *100*, 067205.
40. Liu, Z.; Zhang, S.M.; Yang, J.R.; Liu, J.Z.; Yang, Y.L.; Zheng, Q.S. Interlayer shear strength of single crystalline graphite. *Acta Mech. Sin.* **2012**, *28*, 978–982.
41. Cote, L.J.; Kim, F.; Huang, J. Langmuir- Blodgett assembly of graphite oxide single layers. *J. Am. Chem. Soc.* **2008**, *131*, 1043–1049.
42. Gao, Y.; Cao, T.; Cellini, F.; Berger, C.; de Heer, W.A.; Tosatti, E.; Riedo, E.; Bongiorno, A. Ultrahard carbon film from epitaxial two-layer graphene. *Nat. Nanotechnol.* **2018**, *13*, 133.
43. Elibol, K.; Bayer, B.C.; Hummel, S.; Kotakoski, J.; Argentero, G.; Meyer, J.C. Visualising the strain distribution in suspended two-dimensional materials under local deformation. *Sci. Rep.* **2016**, *6*, 28485.
44. Han, J.; Ryu, S.; Kim, D.K.; Woo, W.; Sohn, D. Effect of interlayer sliding on the estimation of elastic modulus of multilayer graphene in nanoindentation simulation. *EPL (Europhys. Lett.)* **2016**, *114*, 68001.
45. Xiang, L.; Ma, S.Y.; Wang, F.; Zhang, K. Nanoindentation models and Young's modulus of few-layer graphene: A molecular dynamics simulation study. *J. Phys. D Appl. Phys.* **2015**, *48*, 395305.